

A Matched Spectral Benchmark of Quantum Inspired Feature Maps

Toheeb Ogunade¹, Taofeek Kassim², Etinosa Osaro³

¹Department of Computer Science, University of Lagos, Lagos, Nigeria

²Department of Physics, University of Lagos, Lagos, Nigeria

³Department of Chemical Engineering, University of Notre Dame, Indiana, USA

240805099@live.unilag.edu.ng, 230808075@live.unilag.edu.ng, eosaro@nd.edu

Abstract

Quantum machine learning is often motivated by the idea that quantum systems can expose useful high-dimensional structure that is difficult to access with classical models. We isolate one central component of this claim: the fixed data-encoding map. Amplitude, angle, and basis encoding are evaluated as deterministic feature maps for classical supervised learning under matched output dimensionality and strong classical controls. The benchmark compares these encodings against raw linear models, random Fourier features, polynomial features, PCA, RBF SVMs, and shallow neural networks across diverse classical datasets.

Rather than treating performance as a single endpoint, we analyze the geometry of each representation through effective rank, condition number, centered kernel alignment, predictive performance, and practical overhead. The resulting picture is mechanistic: amplitude encoding can remove magnitude information through unit-sphere normalization, angle encoding can become geometrically redundant with raw linear features, and basis encoding can impose a binary Hamming geometry that is poorly aligned with smooth decision structure. These findings do not argue against quantum computation, however, they show that fixed quantum-inspired encoding geometry alone is not a reliable source of machine-learning advantage on classical data.

1 Introduction

Quantum machine learning rests on a powerful premise: quantum systems may represent and manipulate information in feature spaces that are difficult to access classically [1, 2]. Before any trainable circuit, kernel evaluation, or measurement occurs, however, most quantum learning pipelines perform a simpler operation. They encode classical data into a quantum compatible representation. Amplitude, angle, and basis encoding are the standard choices for this step. Each imposes a distinct

geometry on the input data. Amplitude encoding projects samples onto the unit sphere, angle encoding maps features into trigonometric coordinates associated with single qubit rotations, and basis encoding discretises continuous inputs into binary strings.

This paper asks a narrow but important question: does the fixed encoding map itself provide useful representation geometry? The question can be answered without quantum hardware. If amplitude, angle, and basis encoding are implemented as explicit classical feature maps, then their representational value can be tested directly under matched dimensionality, matched data splits, and strong classical controls. Such a benchmark does not decide whether quantum computers can provide advantage. It decides whether one commonly invoked mechanism for advantage, the geometry of the data loading map alone, survives a controlled classical comparison.

The distinction matters. A quantum model may outperform a classical model because of entanglement, measurement statistics, sampling complexity, trainable circuit structure, or data generated by a quantum process. It may also appear to outperform a weak baseline simply because the encoding expands the input dimension. Without isolating the encoding step, these explanations are confounded. A credible claim about quantum machine learning should identify where the advantage enters. This benchmark removes one possible source of ambiguity.

Existing work has shown that quantum kernels can be interpreted through classical kernel theory [2], that classical algorithms can sometimes match proposed quantum speedups under appropriate data access assumptions [3], and that classical models can match quantum kernels on benchmark learning problems when given enough data or suitable inductive bias [4, 5]. These studies motivate a careful separation between the representation induced by a quantum feature map and the broader computational model in which it is deployed. Accuracy alone does not explain why a representation succeeds or fails. It also does not reveal whether an apparent gain comes from useful geometry, increased dimensionality, numerical conditioning, or a weak baseline.

This work evaluates amplitude, angle, and basis encoding as explicit, deterministic feature maps in classical supervised learning. The benchmark spans ten datasets across tabular, image, financial, physics, synthetic, and large scale settings. Each encoding is compared against classical baselines under matched output dimensionality, matched seeds, and comparable optimisation effort. In addition to accuracy and macro F1, we analyse effective rank, condition number, centered kernel alignment, timing, and memory usage.

The result is negative, but it is not merely a negative benchmark. Under matched representational budget, fixed quantum inspired encodings do not produce a statistically significant advantage over strong classical baselines on any dataset tested. Their failures are also predictable. Amplitude encoding fails when normalisation destroys class relevant magnitude structure. Angle encoding is often nearly indistinguishable from the raw linear representation. Basis encoding creates a different representation, but its Hamming geometry is poorly aligned with the smooth decision structure of the benchmark tasks. These findings sharpen the question of quantum advantage rather than dismiss it: the encoding geometry alone is not enough.

The contributions of this paper are as follows:

1. We present a matched benchmark of amplitude, angle, and basis encoding across ten datasets and five independent seeds, compared against strong classical baselines under controlled output dimensionality.
2. We provide a spectral attribution analysis that links performance outcomes to effective rank, condition number, and kernel alignment.
3. We identify three encoding specific failure modes: rank collapse for amplitude encoding, geometric redundancy for angle encoding, and Hamming geometry mismatch for basis encoding.
4. We show that encoding overhead is not the limiting factor. The encodings are computationally cheap, but their induced representations are usually not competitive.
5. We distinguish the scope of the result from claims about quantum hardware. The results rule out fixed encoding geometry as a standalone source of advantage on these classical datasets, but they do not rule out quantum advantage from trainable circuits, entanglement, sampling, or genuinely quantum structured data.

2 Related Work

2.1 Quantum Feature Maps and Quantum Kernels

Quantum feature maps provide a formal route from classical data to quantum Hilbert spaces. A quantum circuit maps input data into a quantum state, and classification can be performed through the induced kernel [1]. Variational quantum circuits can also be interpreted as kernel machines operating in quantum feature spaces [2]. This connection makes quantum learning models analyzable through representation geometry, kernel alignment, and inductive bias. Data reuploading extends this idea by repeatedly injecting classical inputs into parametrised circuits, increasing expressivity even in small quantum systems [6].

2.2 Classical Matching and Dequantisation

Prior work cautions against attributing performance gains to quantum structure without strong classical controls. A quantum inspired classical algorithm can reproduce the speedup of a quantum recommendation algorithm under comparable data access assumptions [3]. In supervised learning, classical models can match quantum models on benchmark datasets when sufficient training data or suitable inductive bias is available [4]. The performance of a quantum kernel also depends strongly on the geometry of the data distribution and the inductive bias induced by the kernel [5]. These findings motivate baselines that control for dimensionality, model family, and tuning effort.

2.3 Limitations of Quantum Machine Learning Models

Quantum learning models also have well documented failure modes. Variational quantum algorithms can suffer from barren plateaus, where gradients vanish rapidly with system size [7]. Quantum neural networks may have large effective dimension, but large capacity does not automatically imply improved generalisation [8]. Quantum kernels can also concentrate, making different samples increasingly similar and reducing discriminative power in high dimensional regimes [9]. Together, these results show that high dimensional quantum representations are not inherently useful. Their geometry must match the task.

2.4 Explicit Feature Maps in Classical Learning

Classical machine learning has long used explicit feature maps to approximate or replace kernels. Random Fourier features approximate shift invariant kernels through random cosine projections [10]. Polynomial expansions, PCA projections, support vector machines, and neural networks provide additional ways to reshape input geometry [11]. This literature makes the central evaluation criterion clear: a feature map is useful only if the similarity structure it induces is aligned with the target function. Dimensional expansion alone is not enough.

2.5 Positioning of This Study

This work does not test quantum hardware and does not resolve the broader question of quantum advantage in machine learning. It isolates one component that appears in many quantum learning pipelines: the fixed encoding map. We implement amplitude, angle, and basis encoding as deterministic feature transformations and compare them against classical alternatives under matched budget. The question is whether the encoding geometry itself is useful. In this benchmark, the answer is no. The spectral analysis explains why.

3 Methods

3.1 Problem Setting

Let $\mathbf{X} \in \mathbb{R}^{n \times d}$ denote a dataset with n samples, d input features, and labels \mathbf{y} . A fixed encoding is a deterministic map

$$\phi : \mathbb{R}^d \rightarrow \mathbb{R}^{d_{\text{out}}}, \tag{1}$$

which transforms each sample before training a downstream classifier. We evaluate whether the encoded representation $\phi(\mathbf{X})$ improves predictive performance relative to classical feature maps of comparable output dimension.

All encodings are fitted only on training data when training statistics are required. The fitted transformation is then applied to the held out test set. No quantum circuit

simulator, quantum measurement routine, or quantum hardware backend is used. The benchmark therefore measures the classical representational effect of the encoding map itself.

3.2 Quantum Inspired Encodings

3.2.1 Amplitude Encoding

For an input vector $\mathbf{x} \in \mathbb{R}^d$, amplitude encoding produces

$$\phi_{\text{amp}}(\mathbf{x}) = \frac{\mathbf{x}}{\|\mathbf{x}\|_2 + \varepsilon}, \quad (2)$$

followed by zero padding to the nearest power of two,

$$d_{\text{out}} = 2^{\lceil \log_2 d \rceil}. \quad (3)$$

The constant $\varepsilon = 10^{-12}$ prevents division by zero. This transformation mirrors the unit norm constraint of quantum state amplitudes. Its central geometric consequence is that all samples are projected onto the unit hypersphere, which removes absolute magnitude information.

3.2.2 Angle Encoding

Angle encoding maps each scaled feature to a pair of trigonometric coordinates motivated by a single qubit rotation:

$$R_y(\theta)|0\rangle = \cos(\theta/2)|0\rangle + \sin(\theta/2)|1\rangle. \quad (4)$$

For classical input data, we implement this as

$$\phi_{\text{ang}}(\mathbf{x}) = [\cos(\theta_1/2), \sin(\theta_1/2), \dots, \cos(\theta_d/2), \sin(\theta_d/2)], \quad \theta_i = \pi \tilde{x}_i, \quad (5)$$

where $\tilde{x}_i \in [-1, 1]$ is obtained by min max scaling using training set statistics. The output dimension is $d_{\text{out}} = 2d$. Each original feature contributes one point on a unit circle.

3.2.3 Basis Encoding

Basis encoding discretises each continuous input feature into an 8 bit integer representation and concatenates the corresponding binary values:

$$\phi_{\text{bas}}(\mathbf{x}) = [b_1^{(1)}, \dots, b_8^{(1)}, b_1^{(2)}, \dots, b_8^{(2)}, \dots] \in \{0, 1\}^{8d}. \quad (6)$$

Here $b_k^{(i)}$ is the k th bit of the quantised value of feature x_i , ordered from most significant to least significant bit. The output dimension is $d_{\text{out}} = 8d$. Unlike amplitude and angle encoding, basis encoding is not differentiable because of the quantisation step.

3.3 Classical Baselines

The benchmark includes classical alternatives designed to test whether QIE performance can be explained by standard feature engineering, dimensional expansion, or model capacity:

- **Raw linear:** standardised input features followed by logistic regression.
- **Random Fourier features:** an explicit approximation to an RBF kernel with output dimension matched to the QIE representation [10].
- **Polynomial features:** degree 2 or degree 3 polynomial expansions when computationally feasible.
- **PCA:** principal component projection with the same target dimensionality as the corresponding encoded representation, capped by the intrinsic rank of the data.
- **RBF SVM:** a radial basis function support vector machine with bandwidth tuned using the training set.
- **MLP baselines:** shallow neural networks implemented in scikit learn and PyTorch, included as adaptive nonlinear baselines.

For each dataset and seed, QIE methods and classical baselines are trained on the same split. Comparisons are made against the best classical baseline observed for that dataset. This is a conservative standard: a fixed encoding is useful only if it can compete with the strongest classical alternative available under the same evaluation protocol.

3.4 Datasets

Table 1 summarises the benchmark suite. The datasets span small tabular classification, imbalanced financial classification, image recognition, high energy physics, synthetic parity, synthetic high rank data, and large scale multiclass classification. The externally sourced datasets are Wine and Breast Cancer from the UCI Machine Learning Repository [12, 13], Dry Bean [14], Credit Card Fraud [15], Fashion MNIST [16], CIFAR 10 [17], HIGGS [18], and Covertypes [19]. The parity and high rank noise tasks are synthetic controls generated by the benchmark code. The dataset roster was fixed before analysing the results.

3.5 Evaluation Protocol

All experiments are repeated over five independent seeds,

$$\{7, 42, 99, 1337, 2026\}. \tag{7}$$

Dry Bean and high-dimensional parity were subsequently extended to ten seeds (adding {100, 200, 300, 400, 500}) after initial results showed large effect sizes that fell short of

Table 1: Benchmark dataset roster.

Dataset	Category	Samples	Features	Classes	Task
UCI Wine	Tabular	178	13	3	multiclass
UCI Breast Cancer	Tabular	569	30	2	binary
Dry Bean	Tabular	13,611	16	7	multiclass
Credit Card Fraud	Financial	284,807	30	2	binary, imbalanced
Fashion MNIST	Image	70,000	784	10	multiclass
CIFAR 10	Image	60,000	3,072	10	multiclass
HIGGS	Physics	500,000	28	2	binary
High dimensional parity	Synthetic	10,000	20	2	binary, XOR
High rank noise	Synthetic	5,000	200	2	binary
Covertypes	Large scale	581,012	54	7	multiclass

$\alpha = 0.05$ under the five-seed design. The same train test split is used for all methods within a given seed. The primary metrics are accuracy and macro averaged F1. Macro F1 is included because accuracy can be misleading on imbalanced datasets, especially Credit Card Fraud.

Statistical significance is assessed using paired tests over all available seeds. For each QIE method and dataset, we compare the seed matched score against the best classical baseline for that dataset. We report paired t test results, Wilcoxon signed rank tests, and Cohen’s d effect sizes. The nominal significance threshold is $\alpha = 0.05$.

To analyse representation geometry, we compute three quantities. First, effective rank is defined as

$$\text{erank}(\mathbf{X}) = \exp\left(-\sum_i \hat{\sigma}_i \log \hat{\sigma}_i\right), \quad (8)$$

where $\hat{\sigma}_i = \sigma_i / \sum_j \sigma_j$ are normalised singular values. Second, the condition number is

$$\kappa(\mathbf{X}) = \frac{\sigma_{\max}}{\sigma_{\min}}, \quad (9)$$

with numerical safeguards for near zero singular values. Third, centered kernel alignment measures similarity between Gram matrices induced by two representations [20]. CKA values near one indicate similar geometry, while values near zero indicate distinct similarity structure.

Table 2: Mean accuracy (up to ten seeds) for QIE encodings and the best classical baseline on each dataset. Bold indicates the highest value in the row. The parity task is marked because all methods remain close to chance.

Dataset	Amplitude	Angle	Basis	Best classical
Wine	0.628	0.972	0.917	0.978 raw linear
Breast Cancer	0.779	0.977	0.940	0.975 PyTorch MLP
Dry Bean	0.260	0.928	0.920	0.931 PyTorch MLP
Credit Fraud	0.999	0.999	0.999	0.999 MLP
Fashion MNIST	0.821	0.823	0.819	0.859 PyTorch MLP
CIFAR 10	0.378	0.306	0.328	0.457 RBF SVM
HIGGS	0.643	0.658	0.669	0.748 PyTorch MLP
High dimensional parity	0.485	0.497	0.504	0.524 PyTorch MLP
High rank noise	0.795	0.780	0.700	0.795 RBF SVM
Covertypes	0.587	0.725	0.724	0.859 MLP

4 Results

4.1 Predictive Performance

Table 2 reports mean accuracy (up to ten seeds) for each QIE method and the strongest classical baseline on each dataset. No QIE method is consistently best. Angle encoding is usually the strongest QIE method on small tabular datasets, but this does not translate into a significant win over classical baselines. Amplitude encoding is highly unstable across datasets and is competitive only on the high rank noise task. Basis encoding performs moderately on several datasets but never surpasses the best classical model.

Across the full benchmark, QIE achieves zero statistically significant accuracy wins against the best classical baseline. Of the 30 encoding-dataset comparisons, 27 are significantly worse at $p < 0.05$ and none are significantly better. The three non-significant cases are genuine negligible near-ties: angle on Wine ($d = -0.18$, $p = 0.70$), angle on Breast Cancer ($d = +0.10$, $p = 0.83$), and amplitude on high-rank noise ($d = -0.03$, $p = 0.96$).

4.2 Macro F1 and Imbalanced Classification

Macro F1 supports the same conclusion as accuracy, but it is more revealing on imbalanced data. On Credit Card Fraud, many methods achieve accuracy near 0.999 because the majority class dominates. Macro F1 separates the models more clearly. The QIE methods achieve macro F1 values of 0.760, 0.845, and 0.887 for amplitude, angle, and basis encoding, respectively, while the strongest neural baselines reach approximately 0.914 to 0.915. Thus, even where QIE appears to match accuracy, it does not match minority class performance.

4.3 Statistical Analysis

Effect sizes confirm that the benchmark outcome is not driven by isolated outliers. Some QIE methods are only slightly below the classical baseline, such as angle encoding on Wine ($d = -0.18$, $p = 0.70$) and angle encoding on Breast Cancer ($d = 0.10$, $p = 0.83$). Other failures are large and systematic. Amplitude encoding on Dry Bean has an effect size of $d = -111.9$ with $p < 0.0001$, and amplitude encoding on Covertypes has $d = -44.0$ with $p < 0.0001$. These extreme cases motivate the spectral analysis in Section 5, which shows that amplitude encoding can collapse the usable rank of the representation.

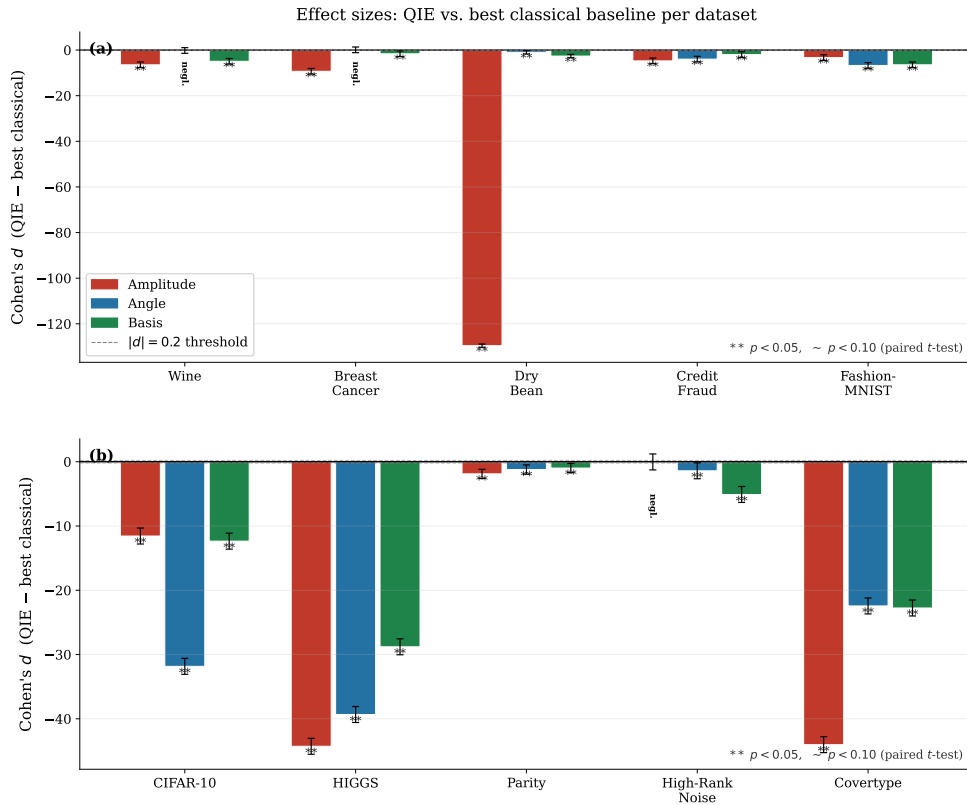


Figure 1: Forest plot of Cohen's d effect sizes for all 30 QIE versus best classical comparisons. Negative values indicate that the QIE method is worse than the best classical baseline. Error bars denote 95% confidence intervals over five to ten seeds.

Table 3: Spectral properties of amplitude encoding on representative datasets. Accuracy gap is measured relative to the best classical baseline.

Dataset	erank	$\log_{10} \kappa$	Accuracy gap
Dry Bean	1.04	9.76	-0.67
Wine	1.38	3.82	-0.35
Breast Cancer	1.64	5.88	-0.20
Covertypes	3.24	5.73	-0.27
High rank noise	197.3	0.35	-0.00

5 Spectral Attribution Analysis

Predictive performance establishes that fixed QIE maps do not outperform the classical alternatives in this benchmark. The more important question is why. We attribute the observed outcomes to three representation level mechanisms: rank collapse, geometric redundancy, and geometry mismatch.

5.1 Amplitude Encoding Collapses Rank When Magnitude Matters

Amplitude encoding projects every sample onto the unit hypersphere. This is faithful to the normalisation requirement of quantum state amplitudes, but it can be harmful for classical data. If class information is partly encoded in vector magnitude, then normalisation removes that signal before the classifier is trained. The result is not merely a small rescaling effect. In several datasets, the encoded matrix becomes nearly rank deficient.

Table 3 shows that the largest amplitude encoding failures coincide with extremely low effective rank and poor conditioning. Dry Bean is the clearest example: amplitude encoding reduces the representation to an effective rank of 1.04 and produces a 67 percentage point accuracy deficit. Wine, Breast Cancer, and Covertypes show the same pattern at smaller scale.

The high rank noise dataset provides an important control. In this case, the data are already distributed in a way that approximately fills the high dimensional sphere. Normalisation therefore does not collapse the representation: $\text{erank} = 197.3$ and $\kappa = 2.22$. Under this condition, amplitude encoding reaches near parity with the best classical method. This supports a falsifiable interpretation: amplitude encoding is competitive only when the original data geometry is already compatible with the unit sphere constraint.

5.2 Angle Encoding Is Often Geometrically Redundant

Angle encoding is the best performing QIE method on several datasets, but CKA shows that this performance usually does not arise from a new representation. Instead, the trigonometric map is often nearly aligned with the raw standardised feature geometry under linear probing.

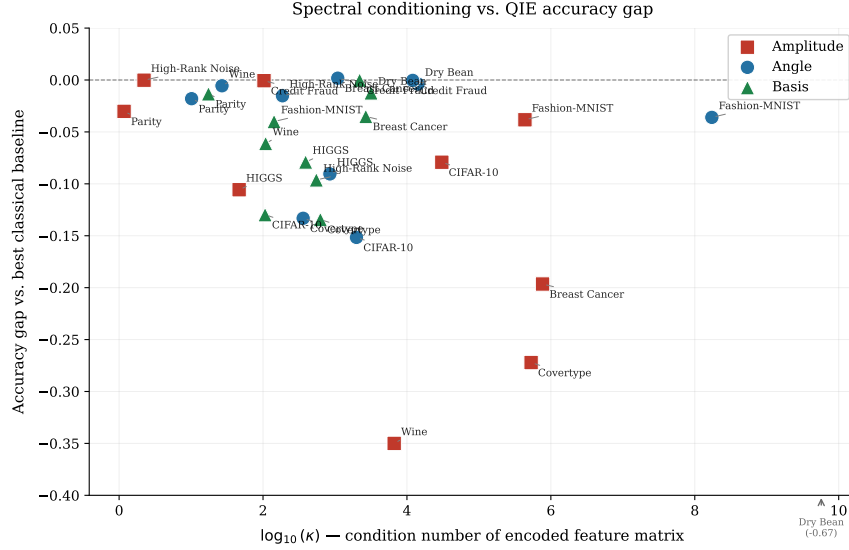


Figure 2: Condition number ($\log_{10} \kappa$) versus accuracy gap (vs. best classical baseline) for all three QIE encodings. Higher condition number is concentrated in amplitude encoding and correlates with larger performance deficits, consistent with the rank collapse failure mode.

On 7 of 10 datasets, $\text{CKA} \geq 0.95$. This indicates that angle encoding induces a Gram matrix that is almost identical to the raw linear representation. In these cases, strong performance should not be interpreted as evidence of a quantum inspired representational advantage. It is better understood as a smooth rescaling of the original features.

The three lower CKA cases, HIGGS, Covertypes, and Credit Fraud, show that angle encoding can become geometrically different from the raw representation. However, it does not become better. This distinction is important: a feature map can be novel without being useful. Angle encoding succeeds when it resembles a classical linear representation and fails to improve when it departs from it.

Table 4: CKA between angle encoded features and raw standardised linear features.

Dataset	CKA(angle, raw linear)
High rank noise	0.985
Fashion MNIST	0.973
Wine	0.971
CIFAR 10	0.971
High dimensional parity	0.968
Dry Bean	0.964
Breast Cancer	0.957
HIGGS	0.636
Covertypes	0.527
Credit Fraud	0.514

space uniformly, the encoding does not destroy information and can match classical performance. When the data do not satisfy this condition, normalisation, redundancy, or binary mismatch dominate.

Table 5: Mean encoding overhead across the ten benchmark datasets.

Method	Enc. time (ms)	Train time (s)	Enc. mem. (MB)	Train mem. (MB)
Amplitude QIE	35.2	13.1	135.7	4.8
Angle QIE	811.3	114.2	291.0	5.6
Basis QIE	1,748	39.6	436.5	345.7
Raw linear	35.2	74.7	47.9	38.0
RFF	193.0	2.1	65.2	24.5
PCA	1,045	14.5	29.1	15.2
Poly 2	10,981	144.9	818.5	178.4

6 Practical Overhead

A possible explanation for poor QIE performance is that the encodings may be too expensive relative to their benefit. The overhead results do not support that explanation. As shown in Table 5, the QIE maps are computationally cheap. Amplitude encoding is essentially as fast as raw standardisation, angle encoding remains below one second on average, and basis encoding is still far cheaper than a degree 2 polynomial expansion.

This is a qualified positive result. If a dataset had geometry well matched to one of these encodings, the transformation would be cheap enough to be useful in practice. The limiting factor in this benchmark is not runtime. It is representational alignment.

7 Discussion

7.1 What the Benchmark Shows

Across ten datasets, fixed quantum inspired encodings do not provide a statistically significant advantage over strong classical baselines. The result is strongest when interpreted mechanistically rather than rhetorically. Amplitude encoding fails when normalisation removes magnitude information and collapses rank. Angle encoding is often competitive only because it closely resembles the raw linear representation. Basis encoding is genuinely different, but its binary geometry is not aligned with the tested tasks.

7.2 What the Benchmark Does Not Show

These results are not an argument against quantum computing. They do not test quantum hardware, entanglement, quantum sampling, trainable variational circuits, or classically hard quantum kernels. The study isolates the encoding step and evaluates it as an explicit classical feature map. The correct conclusion is therefore limited but important: fixed encoding geometry alone is not a sufficient explanation for machine learning advantage on the classical datasets considered here.

7.3 Implications for Quantum Machine Learning

The findings suggest that future claims about quantum machine learning should separate the contribution of the data encoding from the contribution of the trainable or quantum part of the model. If an observed advantage arises from a fixed encoding, it should survive comparison against classical feature maps with matched dimensionality and tuning effort. If it does not, then the advantage must be attributed elsewhere. This separation can make positive claims stronger by eliminating weaker explanations.

7.4 Why Negative Results Matter

A negative benchmark is useful when it narrows the space of plausible mechanisms. In this case, the results show that dimensional expansion, trigonometric lifting, and binary discretisation are not inherently beneficial because they are quantum inspired. The geometry must match the problem. The high rank noise control demonstrates this point directly: amplitude encoding can be competitive when the data distribution satisfies the encoding's assumptions.

7.5 Where Quantum Advantage May Still Appear

The benchmark uses classical datasets. It is possible that quantum structured data, such as molecular quantum states, Hamiltonian spectra, quantum simulation outputs, or problems with provably hard classical representations, could behave differently. It is also possible that learned quantum encodings or entangling circuits could induce

useful structure that fixed encodings do not. These are not contradictions of the present result. They are precisely the settings where future work should look if the fixed encoding map is not enough.

7.6 Limitations

The benchmark evaluates deterministic, parameter free encodings with linear probes and shallow neural baselines. It does not include trainable quantum circuits, data reuploading architectures, hardware noise models, or quantum kernel estimation from finite measurement shots. The number of seeds is sufficient for a controlled benchmark but still modest for very small datasets. Finally, the dataset suite is broad but not exhaustive. The conclusions should therefore be read as evidence against fixed QIE geometry as a general purpose classical feature map, not as a universal statement about all quantum machine learning models.

8 Conclusion

We benchmarked amplitude, angle, and basis encoding as explicit classical feature maps under matched representational budget. Across ten datasets, up to ten seeds, and 30 encoding dataset comparisons, none of the quantum inspired encodings achieved a statistically significant accuracy advantage over the best classical baseline. The failures were not arbitrary. Amplitude encoding often collapsed rank by removing magnitude information. Angle encoding was usually geometrically redundant with raw linear features. Basis encoding produced a distinct but poorly aligned Hamming geometry. Encoding cost was small, so runtime overhead was not the bottleneck.

The broader implication is that fixed quantum inspired encoding geometry, by itself, is not a reliable source of machine learning advantage on classical data. This does not diminish the possibility of quantum advantage from hardware, entanglement, trainable circuits, or quantum structured data. Instead, it clarifies what such an advantage would need to rely on. If quantum machine learning succeeds, the source of the advantage is unlikely to be the fixed encoding map alone.

References

- [1] Vojtěch Havlíček, Antonio D. Córcoles, Kristan Temme, Aram W. Harrow, Abhinav Kandala, Jerry M. Chow, and Jay M. Gambetta. Supervised learning with quantum-enhanced feature spaces. *Nature*, 567(7747):209–212, 2019. doi: 10.1038/s41586-019-0980-2.
- [2] Maria Schuld and Nathan Killoran. Quantum machine learning in feature hilbert spaces. *Physical Review Letters*, 122(4):040504, 2019. doi: 10.1103/PhysRevLett.122.040504.
- [3] Ewin Tang. A quantum-inspired classical algorithm for recommendation systems. In *Proceedings of the 51st Annual ACM SIGACT Symposium on Theory of Computing*, STOC 2019, pages 217–228. Association for Computing Machinery, 2019. doi: 10.1145/3313276.3316310.
- [4] Hsin-Yuan Huang, Michael Broughton, Masoud Mohseni, Ryan Babbush, Sergio Boixo, Hartmut Neven, and Jarrod R. McClean. Power of data in quantum machine learning. *Nature Communications*, 12:2631, 2021. doi: 10.1038/s41467-021-22539-9.
- [5] Jonas M. Kübler, Simon Buchholz, and Bernhard Schölkopf. The inductive bias of quantum kernels. In *Advances in Neural Information Processing Systems*, volume 34, pages 12661–12673, 2021. URL <https://proceedings.neurips.cc/paper/2021/hash/69adc1e107f7f7d035d7baf04342e1ca-Abstract.html>.
- [6] Adrián Pérez-Salinas, Alba Cervera-Liarta, Elies Gil-Fuster, and José I. Latorre. Data re-uploading for a universal quantum classifier. *Quantum*, 4:226, 2020. doi: 10.22331/q-2020-02-06-226.
- [7] M. Cerezo, Andrew Arrasmith, Ryan Babbush, Simon C. Benjamin, Suguru Endo, Keisuke Fujii, Jarrod R. McClean, Kosuke Mitarai, Xiao Yuan, Lukasz Cincio, and Patrick J. Coles. Variational quantum algorithms. *Nature Reviews Physics*, 3:625–644, 2021. doi: 10.1038/s42254-021-00348-9.
- [8] Amira Abbas, David Sutter, Christa Zoufal, Aurelien Lucchi, Alessio Figalli, and Stefan Woerner. The power of quantum neural networks. *Nature Computational Science*, 1:403–409, 2021. doi: 10.1038/s43588-021-00084-1.
- [9] Supanut Thanasilp, Samson Wang, M. Cerezo, and Zoë Holmes. Exponential concentration in quantum kernel methods. *Nature Communications*, 15:5200, 2024. doi: 10.1038/s41467-024-49287-w.
- [10] Ali Rahimi and Benjamin Recht. Random features for large-scale kernel machines. In *Advances in Neural Information Processing Systems*, volume 20, 2007. URL <https://papers.nips.cc/paper/3182-random-features-for-large-scale-kernel-machines>.

- [11] Bernhard Schölkopf and Alexander J. Smola. *Learning with Kernels: Support Vector Machines, Regularization, Optimization, and Beyond*. MIT Press, Cambridge, MA, 2002. ISBN 9780262194754.
- [12] Stefan Aeberhard and M. Forina. Wine. UCI Machine Learning Repository, 1991. URL <https://archive.ics.uci.edu/ml/datasets/wine>.
- [13] William Wolberg, Olvi Mangasarian, Nick Street, and W. Street. Breast cancer wisconsin (diagnostic). UCI Machine Learning Repository, 1995. URL [https://archive.ics.uci.edu/ml/datasets/Breast+Cancer+Wisconsin+\(Diagnostic\)](https://archive.ics.uci.edu/ml/datasets/Breast+Cancer+Wisconsin+(Diagnostic)).
- [14] Murat Koklu and Ilker Ali Özkan. Multiclass classification of dry beans using computer vision and machine learning techniques. *Computers and Electronics in Agriculture*, 174:105507, 2020. doi: 10.1016/j.compag.2020.105507.
- [15] Andrea Dal Pozzolo, Olivier Caelen, Reid A. Johnson, and Gianluca Bontempi. Calibrating probability with undersampling for unbalanced classification. In *2015 IEEE Symposium Series on Computational Intelligence*, pages 159–166. IEEE, 2015. doi: 10.1109/SSCI.2015.33.
- [16] Han Xiao, Kashif Rasul, and Roland Vollgraf. Fashion-mnist: A novel image dataset for benchmarking machine learning algorithms, 2017. URL <https://arxiv.org/abs/1708.07747>.
- [17] Alex Krizhevsky and Geoffrey Hinton. Learning multiple layers of features from tiny images. Technical report, University of Toronto, 2009. URL <https://www.cs.toronto.edu/~kriz/learning-features-2009-TR.pdf>.
- [18] Pierre Baldi, Peter Sadowski, and Daniel Whiteson. Searching for exotic particles in high-energy physics with deep learning. *Nature Communications*, 5:4308, 2014. doi: 10.1038/ncomms5308.
- [19] Jock A. Blackard and Denis J. Dean. Forest coertype. UCI KDD Archive, 1998. URL <https://kdd.ics.uci.edu/databases/coertype/coertype.html>.
- [20] Simon Kornblith, Mohammad Norouzi, Honglak Lee, and Geoffrey Hinton. Similarity of neural network representations revisited. In *Proceedings of the 36th International Conference on Machine Learning*, volume 97 of *Proceedings of Machine Learning Research*, pages 3519–3529. PMLR, 2019. URL <https://proceedings.mlr.press/v97/kornblith19a.html>.

A Supplementary Information

A.1 Reproducibility

All experiments use five fixed seeds, {7, 42, 99, 1337, 2026}. Dry Bean and high-dimensional parity were additionally run on seeds {100, 200, 300, 400, 500} to resolve underpowered comparisons identified in the initial analysis. Code, configuration files, and per seed result files are available at https://github.com/qeinstein/qie_research. Dataset preparation scripts are included for externally sourced datasets. For a fixed seed and software environment, the runner produces deterministic outputs; minor floating point differences may occur across platforms.

A.2 Extended Results

Tables 6 and 7 report mean accuracy and macro F1 across all methods and all datasets. QIE methods are listed first, followed by classical baselines.

Table 6: Mean accuracy and macro F1 for Wine, Breast Cancer, Dry Bean, and Credit Card Fraud.

Method	Wine		Breast Cancer		Dry Bean		Credit Fraud	
	Acc	F1	Acc	F1	Acc	F1	Acc	F1
Amplitude	0.628	0.502	0.779	0.710	0.260	0.059	0.999	0.760
Angle	0.972	0.973	0.977	0.976	0.928	0.939	0.999	0.845
Basis	0.917	0.919	0.940	0.936	0.920	0.931	0.999	0.887
Raw linear	0.978	0.978	0.974	0.972	0.925	0.936	0.999	0.854
RFF	0.889	0.891	0.926	0.920	0.918	0.928	0.998	0.515
PCA	0.928	0.929	0.951	0.947	0.908	0.919	0.999	0.852
Poly 2	0.961	0.961	0.970	0.968	0.927	0.938	0.999	0.903
Poly 3	0.950	0.950	0.958	0.955	0.929	0.940	n/a	n/a
MLP	0.939	0.941	0.956	0.953	0.929	0.940	1.000	0.915
RBF SVM	0.967	0.967	0.972	0.970	0.930	0.941	0.999	0.641
PyTorch MLP	0.961	0.962	0.975	0.974	0.931	0.942	0.999	0.914

Table 7: Mean accuracy and macro F1 for Fashion MNIST, CIFAR 10, HIGGS, high dimensional parity, high rank noise, and Coverttype.

Method	Fashion		CIFAR 10		HIGGS		Parity		High rank noise		Coverttype	
	Acc	F1	Acc	F1	Acc	F1	Acc	F1	Acc	F1	Acc	F1
Amplitude	0.821	0.818	0.378	0.370	0.643	0.637	0.485	0.484	0.795	0.795	0.587	0.213
Angle	0.823	0.824	0.306	0.307	0.658	0.650	0.497	0.496	0.780	0.780	0.725	0.537
Basis	0.819	0.819	0.328	0.326	0.669	0.665	0.504	0.504	0.699	0.699	0.724	0.555
Raw linear	0.797	0.798	0.276	0.275	0.641	0.634	0.486	0.485	0.791	0.791	0.720	0.522
RFF	0.805	0.803	0.362	0.357	0.588	0.576	0.496	0.495	0.696	0.696	0.712	0.503
PCA	0.831	0.830	0.367	0.364	0.614	0.606	0.488	0.486	0.792	0.792	0.671	0.313
Poly 2	n/a	n/a	n/a	n/a	0.679	0.673	0.497	0.497	0.649	0.648	0.765	0.649
MLP	0.854	0.853	0.413	0.413	0.747	0.745	0.500	0.496	0.784	0.784	0.859	0.779
RBF SVM	0.853	0.851	0.457	0.454	0.679	0.674	0.492	0.492	0.795	0.795	0.746	0.493
PyTorch MLP	0.859	0.859	0.432	0.432	0.748	0.747	0.524	0.524	0.777	0.777	0.856	0.780

A.3 Pairwise CKA Among QIE Representations

Table 8 reports pairwise CKA values between the three QIE representations. These values clarify that the encodings are not interchangeable. Amplitude and angle encoding can be closely aligned on some synthetic and physics tasks, while basis encoding is often much more distinct, especially on image datasets.

Table 8: Pairwise CKA between QIE encodings. Values near one indicate similar Gram matrix structure; values near zero indicate geometrically distinct representations.

Dataset	CKA(Amp, Angle)	CKA(Amp, Basis)	CKA(Angle, Basis)
Wine	0.317	0.178	0.433
Breast Cancer	0.561	0.249	0.434
Dry Bean	0.582	0.288	0.448
Credit Fraud	0.166	0.145	0.189
Fashion MNIST	0.740	0.004	0.011
CIFAR 10	0.629	0.001	0.001
HIGGS	0.914	0.581	0.685
High dimensional parity	0.962	0.359	0.358
High rank noise	0.983	0.177	0.190
Coverttype	0.291	0.175	0.887